tablished capability to be functionalized via covalent and noncovalent bonding (*4–6, 9, 10*) opens new strategies for design at the molecular level in areas such as functional membranes and devices based on ionic, electronic, photonic, and control release.

REFERENCES AND NOTES

1. P.-G. de Gennes, *Angew. Chem. Int. Ed. Engl.* **31**, 842 (1992).
2. A. Gaveffotti, *Acc. Chem. Res.* **27**, 309 (1994); J. M. Lehn, *Supramolecular Chemistry* (VCH, Weinheim, Germany, 1995); P. Ball, *Designing the Molecular World* (Princeton Univ. Press, Princeton, NJ, 1994); M. T. Krejchi *et al.*, *Science* **265**, 1427 (1994).
3. A. Keller and G. Goldbeck-Wood, in *Comprehensive Polymer Science*, supplement 2, G. Allen, Ed. (Pergamon, Oxford, 1996), p. 241.
4. N. Ardoin and D. Astruc, *Bull. Soc. Chim. Fr.* **132**, 875 (1995); G. R. Newkome, C. N. Moorefield, F. Vögtle, *Dendritic Molecules* (VCH, Weinheim, Germany, 1996); J. M. J. Fréchet and C. J. Hawker, in (*3*), p. 71.
5. D. A. Tomalia, D. M. Hedstrand, L. R. Wilson, in *Encyclopedia of Polymer Science and Engineering*, Index Volume, H. F. Mark, N. M. Bikales, C. G. Overberger, G. Menges, Eds. (Wiley, New York, ed. 2, 1990), p. 46; J. M. J. Fréchet, *Science* **263**, 1710 (1994); G. R. Newkome *et al.*, *J. Am. Chem. Soc.* **108**, 849 (1986); W. T. S. Huck, B. H. M. Snellink-Ruël, J. W. Th. Lichtenbelt, F. C. J. M. van Veggel, D. N. Reinhoudt, *Chem. Commun.* **1997**, 9 (1997), and references cited therein; P. M. Saville *et al.*, *J. Phys. Chem.* **99**, 8283 (1995); S. S. Sheiko *et al.*, *Macromol. Rapid Commun.* **17**, 283 (1996); I. Gitsov and J. M. J. Fréchet, *J. Am. Chem. Soc.* **118**, 3785 (1996); K. L. Wooley, C. A. Klug, K. Tasaki, J. Schaefer, *ibid.* **119**, 53 (1997).
6. D. A. Tomalia and H. D. Durst, *Top. Curr. Chem.* **165**, 193 (1993); G. R. Newkome *et al.*, *Angew. Chem. Int. Ed. Engl.* **31**, 917 (1992); J. C. M. van Hest, D. A. P. Delnoye, M. W. P. L. Baars, M. H. P. van Genderen, E. W. Meijer, *Science* **268**, 1592 (1995).
7. J. M. Lehn, *Makromol. Chem. Macromol. Symp.* **69**, 1 (1993); E. C. Constable, P. Harverson, M. Oberholzer, *Chem. Commun.* **1996**, 1821 (1996); S. C. Zimmerman, F. Zeng, D. E. C. Reichert, S. V. Kolotuchin, *Science* **271**, 1095 (1996).
8. P.-G. de Gennes and H. Hervet, *J. Phys. Lett.* **44**, L351 (1983); A. M. Naylor, W. A. Goddard III, G. E. Kiefer, D. A. Tomalia, *J. Am. Chem. Soc.* **111**, 2339 (1989).
9. V. Percec, P. Chu, G. Ungar, J. Zhou, *J. Am. Chem. Soc.* **117**, 11441 (1995).
10. V. Percec, G. Johansson, G. Ungar, J. Zhou, *ibid.* **118**, 9855 (1996), and references cited therein.
11. V. S. K. Balagurusamy, G. Ungar, V. Percec, G. Johansson, *ibid.* **119**, 1539 (1997); V. Percec, W.-D. Cho, G. Ungar, V. S. K. Balagurusamy, in preparation.
12. H. Finkelmann, in *Thermotropic Liquid Crystals*, G. W. Gray, Ed. (Wiley, New York, 1987), p. 145; P.-G. de Gennes and J. Prost, *The Physics of Liquid Crystals* (Oxford Scientific, Oxford, 1993); V. Percec, in *Handbook of Liquid Crystal Research*, P. J. Collings and J. S. Patel, Eds. (Oxford Univ. Press, Oxford, 1997), p. 259.
13. E. L. Thomas. D. M. Anderson, C. S. Henkee, D. Hoffman, *Nature* **334**, 598 (1983).
14. Phase transitions in °C and corresponding enthalpy changes in kcal/mol between parentheses are: **1**, k 68 (5.26) Φ_h 78 (0.31) i, i 74 (0.25) Φ_h 0 g; **2**, k 56 (6.19) Φ_h 135 (0.82) i, i 132 (0.83) Φ_h 30 (4.27) k; **3**, k -15 (31.5) Cub 140 (1.63) i, i 127 (1.17) Cub -17 (31.0) k; **4**, k 58 (31.83) Cub 108 (0.41) i, i 99 (0.11) Cub 93 (0.03) k -23 (7.15) k.
15. Planar aligned columnar thin films were obtained by casting a 0.5 wt% toluene solution onto distilled water at a temperature where the monodendron is self-assembled into a supramolecular cylindrical dendrimer. These films were retrieved on copper grids and examined by TEM. Samples of homeotropically aligned supramolecular columnar dendrimers were obtained by annealing thin films supported on carbon. Thin films cast on water were placed on copper grids, coated with carbon, heated to the isotropic phase, and cooled (at 5°C per minute to a particular temperature, before final quenching to 20°C). Films were examined before and after staining with RuO_4 (vapors generated in a closed vessel containing a 0.5 wt% aqueous solution of RuO_4). Brightfield TEM images were obtained with a JEOL 100CX TEM, operated at 100 kV. Thin films of the spherical supramolecular dendrimers were prepared on the same support by cooling at a rate of 0.1°C per minute from 5°C above to 25°C below the isotropization temperature [i in (*14*)].
16. D. M. Walba, F. Stevens, N. A. Clark, D. C. Parks, *Acc. Chem. Res.* **29**, 591 (1996).
17. B. Lotz, *Philos. Trans. R. Soc. London Ser. A* **348**, 19 (1994).
18. L. A. Bumm *et al.*, *Science* **271**, 1705 (1996).
19. P. Oswald and M. Allain, *J. Phys. (Paris)* **46**, 831 (1985).
20. B. Collin, D. Chatenay, G. Coulon, D. Ausserre, Y. Gallot, *Macromolecules* **25**, 1621 (1992); L. H. Radzilowski, B. L. Carvahlo, E. L. Thomas, *J. Polym. Sci. Part B Polym. Phys.* **34**, 3081 (1996); P. Mansky, Y. Liu, E. Huang, T. P. Russell, C. Hawker, *Science* **275**, 1458 (1997); S. I. Stupp *et al.*, *ibid.* **276**, 384 (1997).
21. M. Kleman, in *Points, Lines and Walls* (Wiley, New York, 1983), p. 141.
22. The inclination θ of neighboring columns was measured as a function of z, the distance from the dislocation along the Burger's vector (that is, perpendicular to the central column), and λ was determined most accurately by fitting the equation

$$\theta = \frac{1}{4\sqrt{\pi}} \frac{a}{\sqrt{\lambda z}}$$

23. P.-G. de Gennes and J. Prost, in *The Physics of Liquid Crystals* (Oxford Scientific, Oxford, 1993), pp. 352, 356, and 357.
24. P. M. Wilson and D. C. Martin, *Macromolecules* **29**, 829 (1996).
25. V. Luzzatti, R. Vargas, P. Mariani, *J. Mol. Biol.* **229**, 540 (1993).
26. R. G. Larson, *Chem. Eng. Sci.* **49**, 2833 (1994).
27. The [001] zone axis is typically perpendicular to the film surface, and the ED pattern shown in Fig. 5C [containing the (200) and (210) reflections] was obtained at normal beam incidence. In addition, the following low-angle reflections in the [001] zone were observed: (400), (320), (220) and (310), listed in order of decreasing intensity. At wide angles, a diffuse ring was observed centered at 4.6 Å, indicating that the structure at the atomic level is disordered. The (211) reflection, which is strong and of comparable intensity to the (200) and (210) reflections, can be observed as expected, if the specimen is tilted 27° or 45° about the [100] axis.
28. P. Pradere, J. F. Revol, L. Nguyen, R. S. Manley, *Ultramicroscopy* **25**, 69 (1988).
29. C. Tanford, *Science* **200**, 1012 (1978).
30. ED patterns of unstained samples confirm that only negligible change in the symmetry and dimension of the supramolecular dendrimers and of their LC assemblies results from RuO_4 staining. Identical ED patterns are obtained from unstained samples. However, the material is sensitive to the electron beam, and the low-angle reflections disappear during irradiation, because the electron beam induces structural rearrangements which destroy the order. Stained samples are more resistant to the electron beam.

31. Supported by NSF and the Engineering and Physical Science Research Council, UK.

12 May 1997; accepted 21 August 1997

The Homeotic Gene *lin-39* and the Evolution of Nematode Epidermal Cell Fates

Andreas Eizinger and Ralf J. Sommer*

The fate of ventral epidermal cells differs among nematode species. Nonvulval cells fuse with the epidermis in *Caenorhabditis elegans*, whereas the homologous cells undergo apoptosis in *Pristionchus pacificus*. The homeotic gene *lin-39* is involved in the regulation of these epidermal cell fates. In *Caenorhabditis*, *lin-39* prevents cell fusion of potential vulval cells and specifies the vulva equivalence group. *Pristionchus* vulvaless mutants that displayed apoptosis of the vulval precursor cells were isolated, and point mutations in *lin-39* were identified. Thus, the evolution of these epidermal cell fates is driven by different intrinsic properties of homologous cells.

Evolutionary changes in morphology result from the modification of developmental processes. To study evolutionary transformations in development, it is essential to trace changes in the activity of individual cells and genes. The invariant development of free-living nematodes combined with the genetic and molecular accessibility of some species provide an experimental system in which to study functional alterations in homologous cells and genes during the course of evolution. We analyzed an evolutionary alteration of the fate of homologous ventral epidermal cells among members of two different nematode families.

In the ventral epidermis of *Caenorhabditis elegans*, 12 precursor cells [P1.p through P12.p; denoted as P(1–12).p] adopt either nonvulval or distinct vulval cell fates in a position-specific manner (Fig. 1, A and B) (*1*). The central cells [P(3–8).p], form a so-called vulva equivalence group because all cells have the potential to adopt vulval fates. In the third larval stage (L3), these cells adopt one of three different cell fates.

Max-Planck Institut für Entwicklungsbiologie, Abteilung Zellbiologie, Spemannstrasse 35, 72076 Tübingen, Germany.

*To whom correspondence should be addressed. E-mail: sora@mailer1.mpib-tuebingen.mpg.de

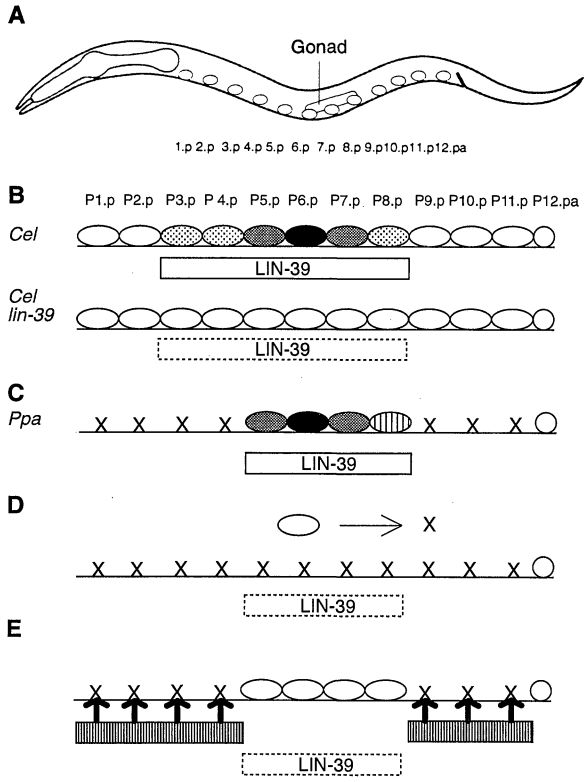

Fig. 1. Schematic summary of the position and the cell fate of ventral epidermal cells. (**A**) In the L1 stage in *Caenorhabditis*, the 12 ventral epidermal cells Pn.p (with n denoting cell number) are equally distributed in the region between the pharynx and the rectum. (**B**) Differentiation pattern of the Pn.p cells in *Caenorhabditis* (*Cel*) (*1*). The nonvulval cells P(1,2,9–11).p (white ovals) fuse with the epidermal syncytium. P12.pa forms hyp12 and is involved in rectum formation. P3.p through P8.p form the vulva equivalence group and adopt one of three alternative cell fates indicated by different symbols (black, cross-hatched, and speckled ovals). The cell denoted by the black oval generates eight progeny, whereas the cells denoted by the cross-hatched ovals generate seven progeny, all of which form part of the vulva. In *lin-39* mutants, P(3–8).p undergo cell fusion like their anterior and posterior lineage homologs (*5*). Wild-type *lin-39* activity is indicated by a solid rectangle, the mutant by a dashed rectangle. (**C**) In *Pristionchus* (*Ppa*), the nonvulval cells P(1–4,9–11).p undergo apoptosis (dead cells denoted as X). P(5–7).p differentiate to form vulval tissue, and P8.p has an epidermal fate (vertical striped oval) (*2, 3*). (**D**) Transformation model: Cell fate is transformed from fusion to death in the evolutionary lineage leading from *Caenorhabditis* to *Pristionchus*. In *lin-39* mutant animals, P(1–11).p should undergo apoptosis. (**E**) Regulation model: Positional information (denoted by striped rectangles) provides an external cell death signal (arrows) that causes apoptosis of P(1–4,9–11).p. A *lin-39* mutation would lead to cell fusion of P(5–8).p (white ovals).

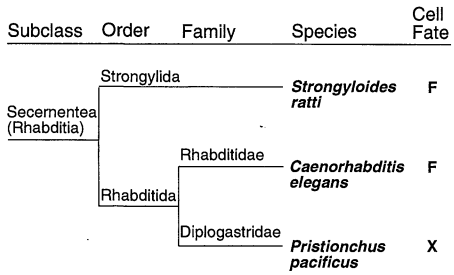

Fig. 2. Proposed phylogenetic relationship between the analyzed species, based on the phylogeny of Malakhov (1994) (*2, 4*). *Strongyloides ratti* of the order Strongylida can be considered as an outgroup for both *Caenorhabditis* and *Pristionchus*. The estimated phylogenetic separation time for *Caenorhabditis* and *Pristionchus* is at least 100 million years (*2, 3*). F, cell fusion; X, cell death.

Table 1. Extent of cell survival and vulva differentiation of VPCs observed in the *Ppa-lin-39* alleles. In the differentiation column, the number of cells that would survive in wild-type animals is given in parenthesis. Although four cells survive in wild type, only three cells are VPCs. n, number of animals analyzed.

Strain	Surviving cells/animals	Differentiated VPCs/surviving VPCs	Animals with induction (%)	*n*
WT	4	150/150 (150)	100	50
sy319	0.01	0/2 (150)	0	50
tu2	0.11	3/3 (165)	5.4	55
tu29	0.81	45/69 (300)	36.0	100
sy374	1.03	64/86 (300)	39.0	100

The nonvulval cells P(1,2,9–11).p in the anterior and posterior region undergo cell fusion with the embryonically derived epidermal syncytium (hyp7) in the first larval stage (L1). In contrast, in *Pristionchus pacificus* (*2, 3*) and other species of the Diplogastridae (*2, 3*), the nonvulval cells [P(1–4,9–11).p] die of programmed cell death, indicating that a change in cell fate specification occurred in the evolutionary lineages of these species (Fig. 1C and Fig. 2) (*4*).

In *Caenorhabditis*, the homeotic gene *lin-39* contributes positional information for the specification of ventral epidermal cells and specifies the six cells P(3–8).p as vulva precursor cells (VPCs) (*5*). In *Caenorhabditis lin-39* mutants, the VPCs undergo cell fusion which results in a vulvaless phenotype (Fig. 1B).

Two models could account for the observed difference in the fate of the nonvulval cells in *Caenorhabditis* and *Pristionchus*. An evolutionary cell-fate transformation from cell fusion to cell death may have resulted in the apoptosis of epidermal cells observed in *Pristionchus* (Transformation model; Fig. 1D). According to this model, *lin-39* promotes vulval cell fate in the central body region and thereby prevents these cells from adopting the default fate (cell death). Alternatively, positional information present only in the anterior and posterior, but not in the central body region, might provide an external cell-death signal which induces the death of P(1–4,9–11).p (Regulation model; Fig. 1E). According to this model, cell fusion would be the default fate of ventral epidermal cells, and positional information in the different body regions would promote cell death and vulval fate, respectively. Thus, *lin-39* would promote vulval cell fate in the central body region and thereby prevents these cells from fusing.

To distinguish between the transformation and the regulation model, we analyzed homeotic mutations in *Pristionchus* that result in a vulvaless phenotype. The two models allow different predictions to be made regarding the fate of the central epidermal cells in a *lin-39* mutant background in *Pristionchus* (Fig. 1, D and E). According to the transformation model, P(5–8).p should undergo apoptosis in *lin-39* mutant animals, whereas the regulation model suggests that a *lin-39* mutation would lead to the fusion of P(5–8).p. Thus, it is possible to distinguish between the two models by the cellular phenotype of mutations in *lin-39*.

We obtained the *Pristionchus* homolog of *lin-39* by polymerase chain reaction (PCR) with degenerate primers within the homeodomain and used this fragment to screen genomic and cDNA libraries (Fig. 3) (*6*). The *lin-39* gene of *Pristionchus* is similar in organization and size to the *lin-39* gene of *Caenorhabditis* but contains one additional intron (Fig. 3A).

From an ethyl methanesulfonate–mutagenesis screen of approximately 40,000 gametes, we isolated more than 50 *Pristionchus* vulva-defective mutants, 17 of which showed a vulvaless phenotype (*7*). By cell lineage analysis, two different phenotypes can be distinguished among the 17 vulvaless mutants. In five mutants, the vulvaless phenotype is caused by the cell death of P(5–

8).p. Complementation analysis revealed that three of these five mutants, *tu2*, *tu29*, and *sy374*, belong to one gene and are all linked to the visible mutation *Ppa-dpy-1*. One mutant, *sy376*, is unlinked to *Ppa-dpy-1* and complements *tu2*, *tu29*, and *sy374* (8). In the 12 other mutants, P(5–8).p survived but did not divide, resembling the phenotype of gonad-ablated wild-type animals (9).

We analyzed the complete *lin-39* coding region and at least 20 base pairs on either side of exon splice sites in the five mutants exhibiting cell death of P(5–8).p and found nonsense mutations in *tu2*, *tu29*, *sy374*, and *sy319* (Fig. 3B) (*10*). In agreement with suggested nomenclature, we named the gene *Ppa-lin-39* (*11*). No mutation was found in *sy376*, which has been named *Ppa-ped-12*.

The vulvaless phenotype of *Ppa-lin-39* is recessive and segregates with normal Mendelian inheritance (*12*). The phenotypes caused by *Ppa-lin-39* mutations were of variable expressivity (Fig. 4 and Table 1). The alleles *sy319* and *tu2* displayed a high penetrance of embryonic and early larval lethality and P(5–8).p underwent programmed cell death in nearly all analyzed mutant animals (Table 1). In contrast, in the two alleles *tu29* and *sy374*, about 30% of the VPCs survived: In 100 *tu29* mutant animals we analyzed, 69 of the potential 300 VPCs survived, 45 of which differentiated into vulval cells later in development. The remaining 24 cells had an epidermal fate and did not divide (Table 1).

The cell-death phenotype of P(5–8).p caused by *Ppa-lin-39* mutations supports the cell fate transformation model, which predicts that cell fusion in *Caenorhabditis* and cell death in *Pristionchus* are alternative nonvulval cell fates. Thus, the difference in cell behavior is an intrinsic property of these cells rather than the result of different external cues. In both species, *lin-39* specifies the central cells to become VPCs and prevents these cells from adopting the nonvulval cell fate. It is unknown however, how *lin-39* regulates this cell-fate decision. Mechanistically, LIN-39 activity might repress the nonvulval fates, promote the vulval fate, or do both. Whereas cell fusion is not very well understood mechanistically, much is known about the mechanisms of cell death in *Caenorhabditis* (*13*). Cell-death mutants have also been isolated in *Pristionchus* (*14*). Such *Pristionchus* cell-death mutants will be useful in studying the link between *lin-39* and apoptosis.

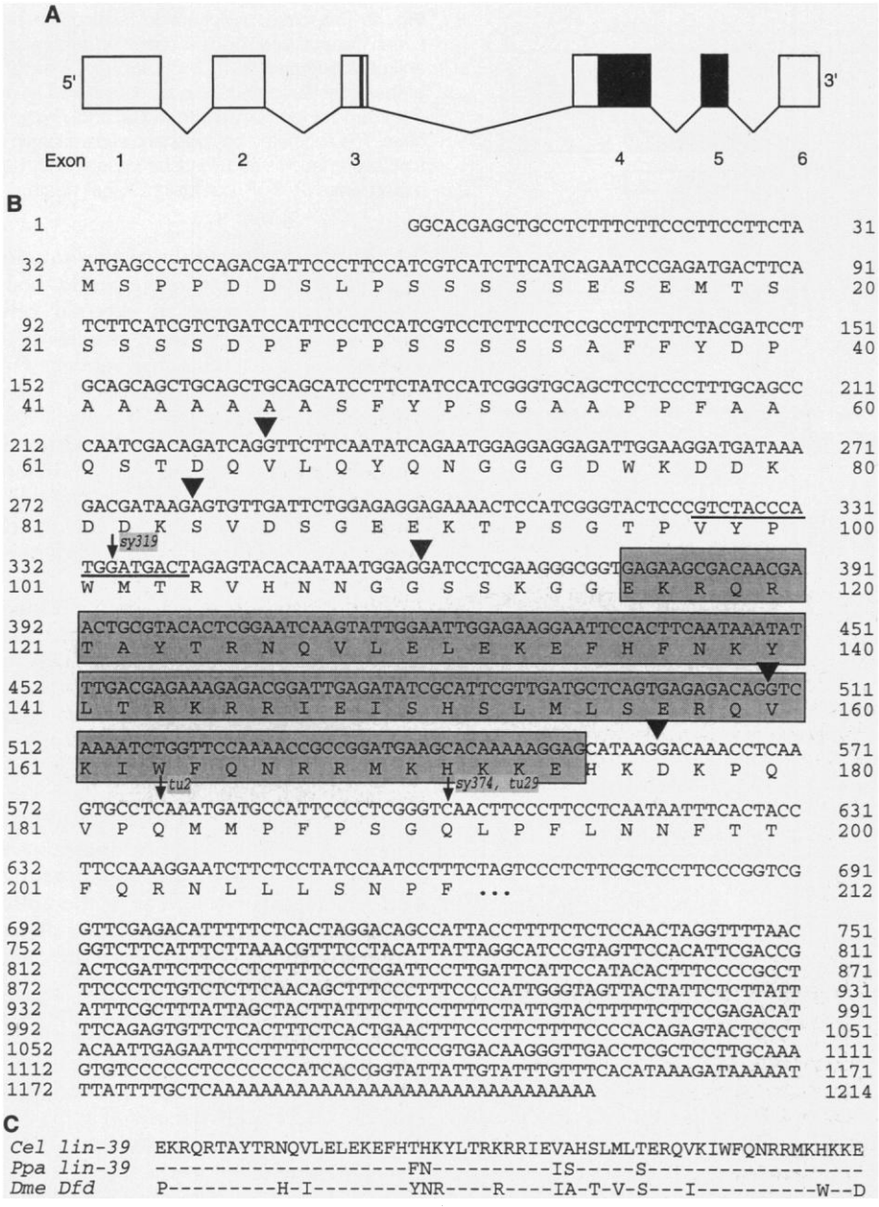

Fig. 3. Cloning and sequencing analysis of *Ppa-lin-39*. (**A**) *Ppa-lin-39* genomic structure. The exact size of intron 3, which is approximately 2 to 3 kb in length (based on Southern hybridization experiments) has not been determined. The hexapeptide and the homeodomain are shown as black boxes. The positions of intron 1, 3, 4, and 5 are conserved between *lin-39* in *Caenorhabditis* and *Pristionchus*. Intron 2 of *Pristionchus* is not present in *Caenorhabditis*. (**B**) Sequence of the longest *Ppa-lin-39* cDNA. Conceptual translation begins with the first in-frame ATG codon. The hexapeptide is underlined and the homeodomain is indicated by a shaded box. Introns are indicated by black triangles. Mutations are indicated by arrows. *sy319* contains a guanine-to-adenine transition, and *tu2*, *tu29*, and *sy374* contain cytosine-to-thymine transitions, all resulting in stop codons. (**C**) Comparison of the homeodomain sequence (*15*) between *Caenorhabditis* (*Cel*) and *Pristionchus* (*Ppa*) *lin-39* and the *Drosophila melanogaster* (*Dme*) *Dfd* gene.

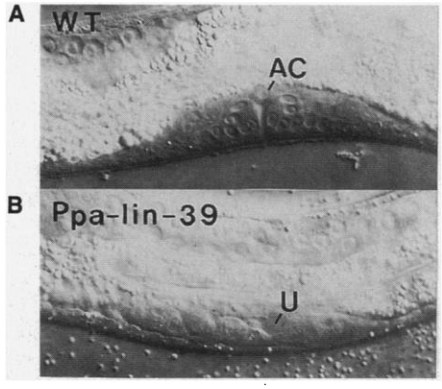

Fig. 4. *Pristionchus lin-39* mutant phenotype. (**A**) Nomarski photomicrographs of a wild-type *Pristionchus* hermaphrodite in the fourth larval stage, showing the seven progeny of P(5,7).p and the anchor cell (AC). (**B**) Nomarski photomicrographs of a *sy319* mutant animal, no vulval cells are present. U, uterus.

REFERENCES AND NOTES

1. J. E. Sulston and H. R. Horvitz, *Dev. Biol.* **56**, 110 (1977).
2. R. J. Sommer and P. W. Sternberg, *Curr. Biol.* **6**, 52 (1996).
3. R. J. Sommer, *Development* **124**, 243 (1997); *Bioessays* **19**, 225 (1997).
4. We would argue that the fusion of nonvulval cells that is seen in *Caenorhabditis* is ancestral, as this cell fate is observed in species of many different families. In particular, *Strongyloides ratti*, a species of the order Strongylida that can be considered as an outgroup for both *Caenorhabditis* and *Pristionchus* [V. V. Malakhov, *Nematodes* (Smithsonian Institution Press, Washington, DC, 1994)] displays fusion of nonvulval epidermal cells (R. J. Sommer, unpublished observation).
5. B. B. Wang *et al.*, *Cell* **74**, 29 (1993); S. G. Clark, A. D. Chisholm, H. R. Horvitz, *Ibid.*, p. 43; S. J. Salser, C. M. Loer, C. Kenyon, *Genes Dev.* **7**, 1714 (1993); T. R. Clandinin, W. S. Katz, P. W. Sternberg, *Dev. Biol.* **182**, 150 (1997).
6. *Ppa-lin-39* was cloned by PCR using degenerate primers in the homeodomain. The primers were 5′-CGTCAGMGTACTGCNTAYAC-3′ and 5′-CATGCKACKRTTYTGRAACCA-3′.
7. Mutagenesis screens were carried out as described (*2*).
8. Hermaphrodites of the fifth mutant, *sy319*, never form ventral protrusions or vulvae and thus, cannot be mated.
9. First genetic characterization of these mutants indicates that they belong to several genes. None of the mutants is linked to *Ppa-dpy-1* (C. Weise and R. J. Sommer, unpublished observation).
10. DNA was isolated from two independent batches of mutant animals, amplified by three independent PCR reactions, and sequenced in both directions. Although the mutant *sy319* cannot be tested genetically, the molecular analysis suggests that the mutant is an allele of *Ppa-lin-39*. The molecular lesion introduces a stop codon into the hexapeptide, removing the complete homeodomain. The strong vulvaless phenotype of *sy319* mutant animals is consistent with the more severe molecular truncation in comparison to the three other alleles (Figs. 3 and 4; Table 1). However, we cannot rule out that a second background mutation is involved in generating the strong vulvaless phenotype of *sy319* mutant animals.
11. D. M. Bird and D. L. Riddle, *J. Nematol.* **26**, 138 (1994).
12. The three alleles *tu2, tu29,* and *sy374* were all marked with the linked recessive visible mutation *Ppa-dpy-1*. Crossed progeny from a mating of such marked vulvaless homozygous hermaphrodites with wild-type males are wild type for the visible marker (being *Ppa-dpy-1*/+) and wild type for the vulva phenotype scored under Nomarski optics (10/10 for each allele). Such heterozygous hermaphrodites segregated one-quarter vulvaless animals, all of which are also homozygous mutant for the visible marker. Segregants that are wild type for the visible marker are also wild type for the vulva phenotype scored under Nomarski optics (25/25 for each allele).
13. J. Yuan, *J. Cell. Biochem.* **60**, 4 (1996).
14. K.-Z. Lee and R. J. Sommer, unpublished observation.
15. Single-letter abbreviations for the amino acid residues are as follows: A, Ala; C, Cys; D, Asp; E, Glu; F, Phe; G, Gly; H, His; I, Ile; K, Lys; L, Leu; M, Met; N, Asn; P, Pro; Q, Gln; R, Arg; S, Ser; T, Thr; V, Val; W, Trp; and Y, Tyr.

16. We thank C. Kenyon and C. Hunter for a *Caenorhabditis lin-39* cDNA clone used in the original hybridization experiments; D. Gilmour, S. Jesuthasan, T. Nicolson, and S. Roth for critical reading of the manuscript; and members of the laboratory for discussion. R.J.S. is a Young investigator with the Max-Planck Society.

11 June 1997; accepted 3 September 1997

Phosphorylation of Sic1p by G_1 Cdk Required for Its Degradation and Entry into S Phase

R. Verma, R. S. Annan, M. J. Huddleston, S. A. Carr, G. Reynard, R. J. Deshaies

G_1 cyclin-dependent kinase (Cdk)–triggered degradation of the S-phase Cdk inhibitor Sic1p has been implicated in the transition from G_1 to S phase in the cell cycle of budding yeast. A multidimensional electrospray mass spectrometry technique was used to map G_1 Cdk phosphorylation sites in Sic1p both in vitro and in vivo. A Sic1p mutant lacking three Cdk phosphorylation sites did not serve as a substrate for Cdc34p-dependent ubiquitination in vitro, was stable in vivo, and blocked DNA replication. Moreover, purified phosphoSic1p was ubiquitinated in cyclin-depleted G_1 extract, indicating that a primary function of G_1 cyclins is to tag Sic1p for destruction. These data suggest a molecular model of how phosphorylation and proteolysis cooperate to bring about the G_1/S transition in budding yeast.

Exit from the G_1 phase and the initiation of DNA synthesis in the cell cycle of budding yeast require the activities of *CDC34*, *CDC4*, *CDC53*, *SKP1*, one member of a set of G_1 cyclin genes (*CLN1-3*), and one member of a set of B-type cyclin genes (*CLB1-6*) (*1–4*). A key insight into the molecular switch that drives cells from G_1 to the S phase was the observation that the G_1/S cell cycle arrest of $cdc34^{ts}$, $cdc4^{ts}$, $cdc53^{ts}$, and $skp1^{ts}$ mutants is suppressed by deletion of *SIC1*, which encodes an inhibitor of the protein kinase activity of a set of S phase–promoting Clb/Cdc28p complexes (*1*, *3*). Biochemical reconstitution experiments have revealed that Cdc4p, Cdc53p, and Skp1p constitute a ubiquitin ligase complex (SCF^{Cdc4}) that collaborates with the ubiquitin-conjugating enzyme Cdc34p and the G_1-specific Cdk Cln2p/Cdc28p (G_1 Cdkl) to promote the ubiquitination of Sic1p (*5*, *6*). Taken together, these data suggest that the destruction of Sic1p via the SCF^{Cdc4} ubiquitination pathway might trigger S phase entry in wild-type budding yeast cells.

G_1 Cdk activity is thought to be required for entry into S phase in all eukaryotic cells, but its exact targets have remained elusive. Sic1p is a potential key substrate of the budding yeast G_1 Cdk, because Cln proteins are required for Sic1p degradation in vivo and ubiquitination in vitro (*2*, *5*), and Cln function is dispensible in cells lacking Sic1p (*2*, *7*). Thus, Cln proteins might trigger Sic1p destruction and entry into S phase by modulating the activity of the Sic1p degradation machinery or by phosphorylating Sic1p directly, thereby allowing it to be recognized as a substrate for proteolysis.

There are nine (Ser or Thr) Pro candidate G_1 Cdk phosphoacceptor sites in Sic1p, seven of which (Fig. 1A) are clustered in the first 105 NH_2-terminal residues. This segment of Sic1p contains sequences that are both necessary and sufficient to specify Cdc34p-dependent ubiquitination (*5*). To test whether Sic1p serves as a substrate for G_1 Cdk, we mixed a purified maltose-binding protein–Sic1p chimera (MBP-$Sic1p^{mycHis6}$; myc and His6 refer to a bipartite epitope tag appended to the COOH-terminus of the hybrid protein) (*8*) with Cln2p/$Cdc28p^{HA}$/Cks1p complexes that were immunoaffinity-purified from insect cell lysates by virtue of the hemagglutinin (HA) tag appended to Cdc28p (*9*). MBP-$Sic1p^{mycHis6}$ was efficiently phosphorylated by eluted G_1 Cdk complexes (Fig. 1B) but not by control eluates prepared from Sf9 cells expressing only Cln2p or Cdc28p. Unfused MBP was not phosphorylated by G_1 Cdk complexes despite its having two potential Cdk phosphorylation sites.

To map the sites at which MBP-$Sic1p^{mycHis6}$ was phosphorylated by G_1 Cdk complexes, we used a multidimensional electrospray mass spectrometry (ESMS) technique (*10–12*). Tryptic phosphopeptides derived from purified phosphorylated MBP-$Sic1p^{mycHis6}$ (Fig. 1C) were isolated by high-performance liquid chromatography (HPLC) followed by ESMS in the negative ion mode through single-ion monitoring of PO_3^-, which has a mass-to-charge ratio (m/z) of 79. The m/z 79 ion is a specific marker for phosphopeptides; the distribution of this ion (Fig. 1D, gray) is superimposed on the 214-nm

R. Verma, G. Reynard, R. J. Deshaies, Division of Biology, Box 156-29, California Institute of Technology, Pasadena, CA 91125, USA. E-mail for R.J.D.: deshaies@cco.caltech.edu

R. S. Annan, M. J. Huddleston, S. A. Carr, Research Mass Spectrometry Laboratory, SmithKline Beecham Pharmaceuticals, King of Prussia, PA 19406, USA.